

Surface freezing in binary mixtures of chain molecules. I. Alkane mixturesE. Sloutskin,¹ X. Z. Wu,² T. B. Peterson,³ O. Gang,^{1,*} B. M. Ocko,⁴ E. B. Sirota,⁵ and M. Deutsch^{1,†}¹*Physics Department, Bar Ilan University, Ramat Gan 52900, Israel*²*San Jose Research Center, Hitachi Global Storage Technologies, 650 Harry Road, San Jose, California 95120, USA*³*Network Data Systems, 1921 Rohlwing Road, Suite D, Rolling Meadows, Illinois 60008, USA*⁴*Physics Department, Brookhaven National Laboratory, Upton, New York 11973, USA*⁵*ExxonMobil Research and Engineering Company, Route 22 East, Annandale, New Jersey 08801, USA*

(Received 16 October 2002; revised manuscript received 5 May 2003; published 23 September 2003)

X-ray surface scattering and surface tension measurements are used to study surface freezing in molten mixtures of alkanes. These binary mixtures consist of protonated and deuterated alkanes, as well as of alkanes of different lengths. As for pure alkanes, a crystalline monolayer is formed at the surface a few degrees above the bulk freezing temperature. The structure of the monolayer has been determined on an angstrom scale. A simple theoretical approach is used to account for the thermodynamical observations at the surface and in the bulk. The model is based on a competition between entropic mixing and a repulsive interaction due to chain-length mismatch. The surface and bulk liquid phases are treated as ideal mixtures, while the solid phases are treated as regular mixtures. The theory is found to account well for all the mixtures studied, both hydrogenated-hydrogenated and hydrogenated-deuterated. The repulsive interaction and its dependence on the chain lengths of the components are determined from fits to the measured data.

DOI: 10.1103/PhysRevE.68.031605

PACS number(s): 61.30.Hn, 68.35.Md, 68.03.Hj, 68.18.Jk

I. INTRODUCTION

Surface freezing (SF) is a first-order formation of a solid layer at the surface of a melt *above* its bulk freezing point [1–4]. With very few exceptions, the opposite effect, surface melting, i.e., the melting of the surface layer *below* the bulk melting point, is the rule in nature, and was observed in metals, semiconductors, polymers, molecular crystals, ice, etc. [5]. Nevertheless, since the discovery of SF in normal alkanes a decade ago [2–4], SF was demonstrated to be the rule, rather than the exception, in chain molecules. SF is exhibited by the simple, purely van der Waals (vdW)-interacting, normal alkanes [$\text{CH}_3(\text{CH}_2)_{n-2}\text{CH}_3$, abbreviated as C_n], by the much more complicated diblock semifluorinated alkanes, by alcohols [$\text{CH}_3(\text{CH}_2)_{n-1}\text{OH}$], which have both hydrogen bonds and vdW interactions, by alkenes, diols, alkyl ethylene glycols, and mixtures and solutions of all these [1–4,6–9]. Binary mixtures of different-length molecules of the same species are of particular interest. By changing the composition and the components' chain lengths, they allow, in principle, the tuning of the bulk free energy continuously over ranges often not accessible in monocomponent melts. The new dimensions provided in phase space by the use of mixtures should generate new phenomena not observed in monocomponent melts. Thus, SF in mixtures is of high importance for fields like wetting, critical phenomena, low-dimensional physics and nanoscience. Moreover, alkanes in “real world” situations, such as lubricants, fuels, etc., occur mostly as mixtures, not as pure compounds. SF in mixtures should be, therefore, of importance also to applied science and industrial applications.

We present here a study of SF in binary mixtures of alkanes. The surface thermodynamics of the melt in its liquid and SF phases was studied by surface tension measurements, and the surface-normal and in-plane structure of the SF layer was studied by surface specific synchrotron x-ray scattering. Its properties and structure, and the effect itself, are strongly dominated by the delicate balance between entropy, which promotes homogeneous mixing, and the repulsion between the two different-length molecules, which promotes segregation of the species. Since the interactions among alkane molecules and their affinity to the surface differ with carbon numbers, the temperature range of the SF effect and the monolayer's structure and composition vary with the carbon number difference Δn . For small- Δn mixtures, the crystalline surface layer is a mixture of the two components. For large Δn , one component of the bulk binary mixture strongly dominates the surface crystalline layer. We have studied extensively two series of mixture, C_{20} with $C_{20+\Delta n}$ and $C_{36-\Delta n}$ with C_{36} where Δn ranges between 2 and 18. The two series show qualitatively similar surface phase behavior with varying Δn .

We have also studied the effects of isotopic substitution on the mixtures, by employing mixtures of protonated (C_n) and deuterated [$\text{CD}_3(\text{CD}_2)_{n-2}\text{CD}_3$, abbreviated here as D_n] alkanes [10]. Here we studied mixtures of D_{32} and C_n , with $n = 20, 23, 26, 32$, and 36 , to investigate the possible influence of isotopic substitution on SF. This effect was shown to be small in the bulk for equal-length molecules [11]. The SF layer, where easy exchange of molecules with the underlying liquid bulk is possible, is a solid where the very slow kinetics of a solid bulk is practically eliminated, and phase separation effects can be studied with practically immediate kinetics. Though the phase diagram of the deuterated materials is generally different from that of their protonated counterparts, we show that the same simple theoretical approach used for the

*Present address: Physics Department, Brookhaven National Laboratory, Upton, NY 11973, USA.

†Corresponding author. Email address: deutsch@mail.biu.ac.il

protonated-protonated mixtures is also valid for the deuterated-protonated ones.

Finally, we also address in this study several theoretical issues concerning SF. Theoretical and simulational models were proposed to explain the SF effect in pure materials [12–16]. A few of these were successful in accounting for the observations [12–14]. However, none of the models allows, even in the simplest cases [12–14], a direct prediction of the SF behavior and properties of binary mixtures. We use here a mean-field thermodynamics approach based on ideal solution theory and the theory of strictly regular mixtures to account for the experimental observations using the properties of the pure components. Only one fit parameter is used, the repulsion energy due to chain-length mismatch, and its behavior is shown to be practically universal, depending only on the chain-length difference between the species.

In Sec. II the experimental details are discussed. Section III presents the thermodynamical theory developed to account for the behavior of the freezing of the bulk and of the surface, along with its very favorable comparison with the measurements. Section IV describes the x-ray surface-diffraction results and their interpretation. The last section, Sec. V, presents our conclusions. A second paper will present a closely related study of SF in alcohol mixtures, as well as conclusions drawn from both studies on the causes, properties and behavior of SF in chain molecules in general.

II. EXPERIMENT

A. Cell and samples

The alkanes were purchased from Cambridge Isotopes (deuterated) and Sigma-Fluka-Aldrich (protonated), were labeled 99% pure, and used as received. The mixtures are prepared by weighing the required amounts into a glass vial, heating to $\sim 10^\circ\text{C}$ above the highest melting point and mixing the melt with a stir bar for half an hour. The well-mixed sample is then poured onto a preheated silicon substrate and sealed in a temperature regulated cell. The experimental results are mostly independent of the thermal cycle when cooled below bulk freezing and reheated. Nevertheless, the results discussed below are those obtained in the first cooling cycle of the mixed melt.

B. Surface tension measurements

The surface tension (ST) γ was measured using the Wilhelmy plate method [17]. The Wilhelmy plate was made of filter paper to enhance wetting by the alkane sample [18]. The ST is a direct measure of the surface excess free energies: $\gamma = \epsilon^s - \epsilon^b - T(S^s - S^b)$, where ϵ^s and ϵ^b are the energies and S^s and S^b are the entropies of the surface and the bulk, respectively. The surface tension temperature scans for several $\text{C}_{20} + \text{C}_{26}$ mixtures are shown in Fig. 1. The first-order surface freezing transition is directly manifested by a sharp change in the slope of the surface tension, $d\gamma/dT = -S^s + S^b$, from a small negative value for the $T > T_s$ liquid surface phase to a large positive value for the $T < T_s$ crystalline surface phase [1,4,18]. The variation of the SF onset temperature $T_s(\phi)$ with the concentration of the high mo-

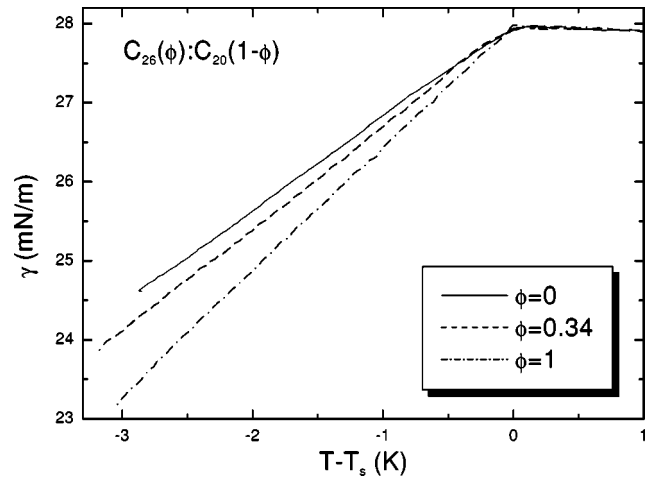


FIG. 1. Several typical surface tension (γ) temperature scans of $\text{C}_{20} + \text{C}_{26}$ alkanes are shown for the liquid bulk concentrations (ϕ) listed. The curves end at the bulk freezing temperatures. Since the measurement errors in the absolute surface tension values are no better than ~ 1 mN/m, all curves were shifted by small amounts to make them coincide at T_s , to enhance presentation clarity. The T_s values of the curves shown are $T_s = 38.6, 46.5,$ and 58.6°C , for $\phi = 0, 0.34,$ and 1 , respectively.

lecular weight species, ϕ , was determined from temperature scans of the surface tension $\gamma(T)$. At some temperature below T_s strong fluctuations occur in the force exerted by the sample on the Wilhelmy plate. These fluctuations mark the onset of bulk freezing $T_f(\phi)$. As earlier studies show [18], even in materials that do show supercooling of the bulk freezing transition, the Wilhelmy plate acts as a nucleator and the temperature range of supercooling is significantly reduced. Preliminary bulk calorimetry measurements indicate a possible lack of bulk supercooling in melts of binary alkane mixture when the components do not differ much in length. Thus, at least for mixtures of small chain-length mismatch, $\Delta n/\bar{n} = (n_1 - n_2)/[(n_1 + n_2)/2]$, one may equate the onset temperature of the Wilhelmy plate fluctuations with the thermodynamical-equilibrium bulk freezing point T_f . The surface entropy loss upon SF [1,4], ΔS^s , can be obtained from the surface tension scans (in Fig. 1), as $\Delta S^s = d\gamma/dT|_{T < T_s} - d\gamma/dT|_{T > T_s}$. Note, however, that these values are given *per unit area*, same as γ , rather than *per molecule* [18]. Since, to the best of our knowledge, no direct measurement of the molecular area in the *liquid* surface layer is available in the literature, we cannot use the measured surface ΔS^s to obtain the entropy loss at the surface *per molecule*. Rather, we use the measured *bulk* entropy loss upon SF, ΔS^b , which is known from earlier calorimetric studies [1,19] in units of J/(K mol), to derive the entropy loss per molecule, and use this value for both surface and bulk freezing. The consistent results obtained using values calculated this way support the validity of the assumption of nearly identical entropy loss *per molecule* upon freezing at the surface and in the bulk [1].

C. X-ray methods

The structure of the vapor-liquid interface of the melt has been studied by x-ray reflectivity (XR) and x-ray grazing

incidence diffraction (GID). The reflectivity $R(q_z)$, where $q_z = (4\pi/\lambda)\sin\alpha$ is the surface-normal momentum transfer, α is the angle of incidence of the x-ray beam and $\lambda \approx 1.5 \text{ \AA}$ is the wavelength of synchrotron radiation used, yields information on the electron density profile normal to the surface, and allows accurate measurement of the thickness and electron density of a surface-frozen layer [20,21]. For an ideally smooth and abrupt surface separating two media of different constant densities, the reflectivity is known as the Fresnel reflectivity [22],

$$R_F(q_z) = \left| \frac{q_z - \sqrt{q_z^2 - q_c^2}}{q_z + \sqrt{q_z^2 - q_c^2}} \right|^2, \quad (1)$$

where $q_c \approx 0.02 \text{ \AA}^{-1}$ corresponds to the critical angle of incidence, α_c , below which total reflection of the impinging x rays occurs. R_F falls off monotonically as $(2q_c/q_z)^4$ for $q_z \gtrsim 4q_c$. A real-world interface is seldom abrupt, or ideally smooth, and its x-ray reflectivity is given by

$$\frac{R(q_z)}{R_F(q_z)} = \left| \int \frac{1}{\rho_{bulk}} \frac{d\langle\rho(z)\rangle}{dz} e^{iq_z z} dz \right|^2, \quad (2)$$

where $\rho(z)$ is the electron density variation with depth z below the surface, and the density averaging $\langle \dots \rangle$ is done in the surface parallel plane [20]. Approximating the electron density profile by a sum of $N+1$ slabs of fixed densities ρ_i , $R(q_z)/R_F(q_z)$ can be modeled as

$$\frac{R(q_z)}{R_F(q_z)} = \left| \sum_{i=0}^N \left(\frac{\rho_i - \rho_{i+1}}{\rho_{bulk}} \right) e^{-iq_z D_i} e^{-iq_z^2 \sigma_{i+1}^2 / 2} dz \right|^2, \quad (3)$$

where i sums over $N+1$ layers, D_i is the distance of the i th interface from the bulk, σ_i is the width of the Gauss-distributed interfacial roughness, $\rho_0 = \rho_{bulk}$, and $\rho_{N+1} \approx 0$ is the electron density of the vapor. For the alkane melt's surface in the SF phase, a two-slab ($N=2$) model can be used. The upper slab represents the $(\text{CH}_2)_{n-2}$ alkyl chain and the lower slab represents the smaller density CH_3 methyl group at the monolayer-bulk interface. The slab of the second methyl groups at the monolayer-vapor interface is included in the roughness of the interface. This model was used successfully to represent the density profile of the SF phase of pure alkane melts [1,3] and alkane-containing solutions [18]. The densities, thicknesses, and interfacial roughnesses of all layers are refined in the fit to yield the best fit of the model to the experimental reflectivity curve, $R(q_z)$. To reduce the number of fit parameters, all interfaces were assumed to have the same roughness σ . In our two-slab model this practice results in five fit parameters: two thicknesses, two densities, and one roughness parameter.

The in-plane structure of the SF monolayer is probed by x-ray GID [20,23]. Here, the incident angle is set to $\alpha < \alpha_c$, so that total external reflection of the impinging x rays occurs, yielding an evanescent wave, which travels along the

surface and penetrates the surface layer to a depth of $\sim 75 \text{ \AA}$. Scanning the detector horizontally at an angle θ_D relative to the specular reflection plane, the intensity diffracted out of the evanescent wave by the crystalline structure of the surface is measured as a function of the in-plane momentum transfer $q_r = (4\pi/\lambda)\sin(\theta_D/2)$ [1,20,23]. This GID diffraction pattern can be analyzed by standard crystallographic techniques to yield the in-plane structure. In particular, for an hexagonal packing of the molecules in the SF layer, the nearest-neighbor separation is given by $a = 2\pi/[q_r \cos(30^\circ)]$, where q_r is the peak position of the single GID peak observed in this case. Finally, the magnitude and direction of the tilt of the SF layer's molecules can be deduced from the Bragg Rods (BR)—the surface-normal intensity distribution, measured at the in-plane GID peak positions [1,20,23]. The three scans, XR, GID, and BR, allow a complete determination of the in-plane and surface-normal structure of the SF monolayer.

III. RESULTS: THERMODYNAMICS

We present here the results of the surface tension measurements on the various binary alkane mixtures studied and the thermodynamical theory that explains their behavior in terms of the pure components' properties. For samples where the length mismatch of the two components is small, a "mixture model" was employed, in which the free energy of the solid phase includes entropic and enthalpic terms to account for the mixing. For samples where the length mismatch is large, a "solution model" was used, in which a single-component solid phase is assumed and thus the free energy does not include mixing terms. The measured quantities used in the analysis and figures discussed below are listed in Tables I and II.

A. Basic theory of alkane mixtures

The behavior of the surface phase can be accounted for, in general, using the properties of pure components and taking into consideration the mixing entropy and the molecular interactions [24–26]. The liquid phase of a binary alkane mixture can be treated as an ideal mixture, since chain-length mismatch is irrelevant in the liquid phase, where most of the molecules are kinked and no long-range positional order exists. Thus, the free energy of a bulk comprising N molecules of C_n and M molecules of C_m can be written as [24,25,27]

$$F^{lb} = Nf_n^{lb} + Mf_m^{lb} + k_B T \left[N \ln \frac{N}{N+M} + M \ln \frac{M}{N+M} \right], \quad (4)$$

where $f_i^{lb} = \epsilon_i^{lb} - TS_i^{lb}$ is the bulk free energy of a molecule in a liquid melt of pure C_i , ϵ_i^{lb} is its energy, and S_i^{lb} is its entropy, with $i = n, m$. The last term is the mixing entropy due to the additional $(N+M)!/(N!M!)$ distinguishable states in a binary mixture as compared to a pure material. The chemical potentials of C_n and C_m are given by $\mu_n^{lb} = \partial F^{lb}/\partial N$ and $\mu_m^{lb} = \partial F^{lb}/\partial M$.

TABLE I. Thermodynamical data obtained by surface tension measurements. ϕ is the mole fraction of the long-chain species in the bulk liquid, T_s is the surface freezing temperature, T_f is the bulk freezing temperature, and ΔS^s is the entropy loss, per unit area, upon surface freezing. For $C_{32}+D_{32}$, ϕ is the protonated alkane fraction.

ϕ	T_f (°C)	T_s (°C)	ΔS^s (mJ/[m ² K])	ϕ	T_f (°C)	T_s (°C)	ΔS^s (mJ/[m ² K])
		$C_{28}+C_{36}$				$C_{30}+C_{36}$	
1	74.55	77.1	1.84	1	74.73	77.33	1.85
0.7	70.86	73.43	1.88	0.69	71.91	74.42	1.83
0.44	66.56	69.33	1.86	0.44	69.04	71.7	1.79
0.3	63.94	66.86	1.67	0.23	66.33	69.32	1.72
0.18	62.06	65.18	1.55	0	64.62	67.42	1.63
0	60.08	63.17	1.55				
		$C_{20}+C_{24}$				$C_{20}+C_{22}$	
1	49.94	52.98	1.40	1	43.51	46.6	1.20
0.66	45.39	48.59	1.36	0.73	41.26	44.55	1.18
0.45	42.17	45.41	1.33	0.55	39.95	43.31	1.13
0.18	37.37	41.0	1.22	0.39	38.24	41.86	1.16
0.06	35.98	39.39	1.20	0.23	37.27	40.64	1.12
0	35.68	38.61	1.17	0	35.68	38.83	1.07
		$C_{20}+C_{25}$				$C_{20}+C_{26}$	
1	53.01	56.05	1.45	1	55.66	58.63	1.42
0.67	48.3	51.48	1.45	0.7	50.91	53.94	1.43
0.48	45.93	49.11	1.48	0.41	44.66	47.73	1.39
0.43	41.87	45.12	1.37	0.3	41.66	44.86	1.29
0.33	40.18	43.67	1.30	0.14	37.04	40.99	1.14
0.24	38.7	42.36	1.77	0	35.63	38.65	1.05
0.15	37.0	40.88	1.20				
0.07	36.07	39.91	1.16				
0	35.63	38.65	1.15				
		$C_{32}+C_{36}$				$C_{20}+C_{30}$	
1	74.6	77.09	1.84	1	64.62	67.42	1.63
0.84	73.52	76.18	1.87	0.8	61.95	64.59	1.69
0.77	72.86	75.51	1.84	0.67	59.26	62.04	1.75
0.67	72.33	75.02	1.81	0.53	57.51	59.27	1.75
0.47	71.11	73.83	1.76	0.45	55.98	56.96	1.70
0.24	69.76	72.21	1.76	0.38	54.5		
0.12	68.76	71.78	1.77	0.15	47.1		
0.06	68.65	71.54	1.72	0.08	42.2		
0.05	68.52	71.36	1.72	0.03	35.75	39.27	1.09
0	68.3	70.64	1.73	0	35.63	38.65	1.05
		$C_{20}+C_{28}$				$C_{36}+D_{32}$	
1	60.5	63.6	1.50	1	74.8	77	2.03
0.74	57.9	60.05	1.50	0.95	74.29	76.84	1.99
0.66	54.84	57.39	1.74	0.9	73.88	76.33	2.0
0.5	52.6	55.2	1.54	0.8	72.97	75.27	1.96
0.42	51.16	52.7	1.72	0.7	72.08	74.02	2.01
0.41	48.3	49.41	1.42	0.6	71.15	72.44	2.08
0.26	44.5	45.14	1.56	0.5	69.68	70.94	1.97
0.23	44.88	45.42		0.41	68.67	70.07	2.06
0.21	42.3	43.1	1.11	0.4	68.58	69.6	2.05
0.17	40.1	41.93	1.09	0.30	67.26	68.98	2.0
0.16	41.44	42.11		0.20	65.79	67.67	1.95
0.13	38.6	41.3	1.08	0.15	65.24	66.72	1.89
0.11	40.36	41.25	1.09	0.102	64.5	66.05	1.90
0.1	36.8	40.6	1.05	0.101	64.49	66.52	1.60
0.09	35.8	40.05	1.11	0.068	64.0	65.52	1.96

TABLE I. (Continued).

ϕ	T_f (°C)	T_s (°C)	ΔS^s (mJ/[m ² K])	ϕ	T_f (°C)	T_s (°C)	ΔS^s (mJ/[m ² K])
0.07	35.35	39.78	1.11	0.05	63.65	65.35	1.94
0.05	35.3	39.45	1.08	0	63.3	65.9	1.8
0	35.71	38.75	1.08				
		C ₂₀ +D ₃₂				C ₃₂ +D ₃₂	
1	35.54	38.54	1.14	1	68.57	71.32	1.7
0.97	35.05	38.69	1.08	0.91	68.13	70.77	1.64
0.96	35.12	38.82	1.17	0.87	67.94	70.47	1.72
0.94	38.57	38.9	1.97	0.83	67.72	70.32	1.67
0.88	43.87			0.76	67.4	69.79	1.65
0.81	48.26			0.73	67.25	69.81	1.75
0.73	51.18			0.69	66.96	69.33	1.69
0.65	54.56			0.63	66.8	69.36	1.77
0.55	55.46			0.53	66.35	69.0	1.74
0.44	57.66	58.53	1.04	0.43	65.89	68.5	1.74
0.31	59.15	60.4	1.88	0.33	65.21	67.85	1.78
0.17	61.11	62.91	1.83	0.23	64.67	67.33	1.76
0.05	62.55	64.42	1.85	0.11	64.09	66.67	1.73
0	63.3	65.9	1.8	0	63.3	65.9	1.8
		C ₂₃ +D ₃₂				C ₂₆ +D ₃₂	
1	46.77	49.85	1.34	1	55.4	58.04	1.52
0.97	46.46	50.0	1.35	0.93	55.43	58.11	1.53
0.91	46.36	50.22	1.38	0.85	55.62	58.66	1.58
0.86	46.64	50.4	1.39	0.77	56.14	59.22	1.63
0.83	47.26	50.71	1.40	0.68	56.74	59.7	1.63
0.79	48.34	51.0	1.46	0.59	57.48	60.12	1.67
0.75	50.5	52.17	1.53	0.38	59.3	61.69	1.74
0.71	52.14	52.9	2.0	0.26	60.61	62.9	1.86
0.62	54.52	55.47	1.97	0.14	61.9	64.08	1.83
0.57	55.1	56.42	1.86	0	63.3	65.9	1.8
0.46	57.23	58.6	1.97				
0.35	58.45	60.1	1.9				
0.25	59.89	61.4	1.83				
0.15	61.2	62.39	1.89				
0.08	62.03	63.35	1.8				
0	63.3	65.9	1.8				

In the crystalline phase, ordered layers are formed in which all chains are extended and aligned parallel to one another. The crystal can then be regarded as mixture of cylinders with similar diameters but different lengths. In this case, the mixture can no longer be considered ideal, since exchanging a single molecule between pure C_m and C_n crystals raises their total energy by twice the interchange energy, ω_b [24,25]. Since each molecule interacts with its $z=6$ nearest neighbors (in the layer plane), the energy of a nonidentical pair is increased by $2\omega_b/z$, compared to an identical pair. The free energy of the crystalline phase is then [24,25,27–29]

$$F^{cb} = Nf_N^{cb} + Mf_M^{cb} + k_B T \left[N \ln \frac{N}{N+M} + M \ln \frac{M}{N+M} \right] + \omega_b \frac{NM}{N+M}, \quad (5)$$

where $f_i^{cb} = \epsilon_i^{cb} - TS_i^{cb}$ is the bulk free energy of a molecule in a crystal of pure C_i ($i=n,m$). The third term is, again, the mixing entropy. The last term in Eq. (5) is the interchange energy in the zeroth-order approximation to the “strictly-regular” mixture theory [25]. It consists of ω_b times the probability of occurrence of a nonidentical pair in a randomly mixed binary mixture, neglecting higher-order interactions [24,25]. The chemical potentials are obtained, again, as $\mu_n^{cb} = \partial F^{cb} / \partial N$ and $\mu_m^{cb} = \partial F^{cb} / \partial M$. The last, repulsive, term in Eq. (5) favors phase separation, whereas the mixing entropy term favors a homogeneously mixed phase [30]. When $2k_B T > \omega_b$, the mixing entropy is dominant and a homogeneously mixed crystalline phase may exist at any mole fraction x . However, when $2k_B T < \omega_b$, the repulsive interaction dominates for compositions x close to equimolar, and phase separation will occur for these x in the crystalline phase [28].

TABLE II. Same as Table I above, but for the mixtures $C_{25}+C_{36}$ and $C_{26}+C_{36}$. These have an additional transition, at the edge of the black hole region, as discussed in the text, to a phase with a different tilt and higher entropy loss (higher ΔS_i) than at the usual surface freezing (ΔS^s). For some compositions the transition occurs at $T_{tr} < T_s$. For others, the SF transition at $T = T_s$ is directly to the anomalous SF phase [8].

$C_{25}+C_{36}$						$C_{26}+C_{36}$					
ϕ	T_f	T_s	ΔS^s	T_{tr}	ΔS_i	ϕ	T_f	T_s	ΔS^s	T_{tr}	ΔS_i
1	74.73	77.33	1.85			1	74.73	77.33	1.85		
0.57	69.43	70.96	1.99	69.67		0.68	70.66	72.93	1.95		
0.52	68.42	69.67	1.91	69.36	2.81	0.57	69.33	71.06	1.98		
0.43	66.83	68.03			3.05	0.52	68.14	69.72	2	68.74	3.08
0.35	65.72	66.46			2.9	0.45	67.7	69.18	1.96	68.55	2.84
0.15	59.2	59.54	2.4			0.42	66.6	68.01			2.85
0.08	53.15	56.91	1.348			0.3	64.3	64.6			
0	52.81	55.97	1.36			0.24	62.75	62.98			
						0.17	60.7	60.7			
						0.14	58.41	60	1.51		
						0.12	56	59.59	1.49		
						0.07	55.62	59.42	1.46		
						0	55.66	58.63	1.42		

B. Results for the bulk

At the bulk solid-liquid transition, the solid crystal phase coexists with the liquid phase, each component having the same chemical potential in the two phases. Equating the relevant chemical potentials yields

$$f_n^{lb} + k_B T \ln \phi = f_n^{cb} + k_B T \ln x_b + \omega_b (1 - x_b)^2, \quad (6)$$

$$f_m^{lb} + k_b T \ln(1 - \phi) = f_m^{cb} + k_B T \ln(1 - x_b) + \omega_b x_b^2. \quad (7)$$

Here the left-hand sides are the chemical potentials μ_n^{lb} (μ_m^{lb}) of the C_n (C_m) molecules in the liquid bulk and the right-hand sides are the chemical potentials μ_n^{cb} (μ_m^{cb}) of the C_n (C_m) molecules in the crystalline bulk phase. $\phi = N/(N + M)$ is the mole fraction of the C_n molecules in the liquid bulk and x_b is the mole fraction of the same molecules in the crystalline bulk. It is important to note that, in general, x_b differs from ϕ . The free energy difference $f_i^{cb} - f_i^{lb}$ of each component can be derived from the pure component's bulk freezing temperature $T_{f,i}$ and the latent heat $\epsilon_i^{lb} - \epsilon_i^{cb} = T_{f,i}(S_i^{lb} - S_i^{cb})$, using $f_i^{cb} - f_i^{lb} = (T - T_{f,i})(S_i^{lb} - S_i^{cb}) = (T - T_{f,i})\Delta S_i^b$, where ΔS_i^b denotes the entropy loss upon bulk freezing of a single C_i molecule. Using these, Eqs. (6) and (7) yield

$$T_f(\phi) = [T_{f,n}\Delta S_n^b - \omega_b(1 - x_b)^2] / [\Delta S_n^b + k_B \ln(x_b/\phi)], \quad (8)$$

$$T_f(\phi) = (T_{f,m}\Delta S_m^b - \omega_b x_b^2) / \{\Delta S_m^b + k_B \ln[(1 - x_b)/(1 - \phi)]\}. \quad (9)$$

The entropy loss upon bulk freezing, ΔS_i^b , and the bulk freezing temperatures $T_{f,i}$ of the pure components are known

from previous measurements [1,19]. Using these, Eqs. (8) and (9) can be solved by fitting them to the bulk freezing temperatures measured as a function of concentration, $T_f(\phi)$, for a given mixture. This yields the solid bulk compositions $x_b(\phi)$ and the interchange energy ω_b . Note that the freezing temperature is, by definition, the temperature at which the first solid grain is nucleated within the liquid bulk. The volume of this grain is, however, very small, so that its composition $x_b \neq \phi$ does not change the actual remaining liquid composition ϕ from the nominal ϕ_0 . However, as the temperature is reduced, the solid fraction grows, and the composition ϕ will increasingly deviate from the nominal ϕ_0 . The whole process obeys Eqs. (8) and (9) at any given temperature, implying that T_f in these equations is not the single freezing temperature, but a particular solid-liquid coexistence temperature out of a range of temperatures in the vicinity of the rigorous freezing temperature. The experimentally observed transition is sharp, proving this range to be small [31]. Each T_f corresponds to some $\phi \neq \phi_0$ through Eqs. (8) and (9). Experimentally, of course, only ϕ_0 can be controlled independently.

The results obtained using the theory above for a mixture of two close-length alkanes are shown in Fig. 2. Good fit (dashed line) to the measured T_f values (closed squares) in Fig. 2(b) is obtained, supporting the applicability of the theory above in this case. The solid composition x_b is found to deviate from the nominal liquid composition, ϕ , by up to $\sim 15\%$, as shown in dashed line in Fig. 2(a). Note that the two components of these mixtures have almost equal lengths, differing only by ~ 2.5 Å. Thus, ω_b is small and so is the repulsive mismatch term in Eq. (5). This, in turn, results in the dominance of the mixing entropy at all compositions, and a continuous composition curve $x_b(\phi)$ is obtained, deviating only slightly ($\approx 15\%$) from ϕ , as shown in dashed line in Fig. 2(a). When the chain-length mismatch is large, as for the $C_{26}+C_{36}$ mixture shown in Fig. 3, $x_b(\phi)$ deviates from ϕ

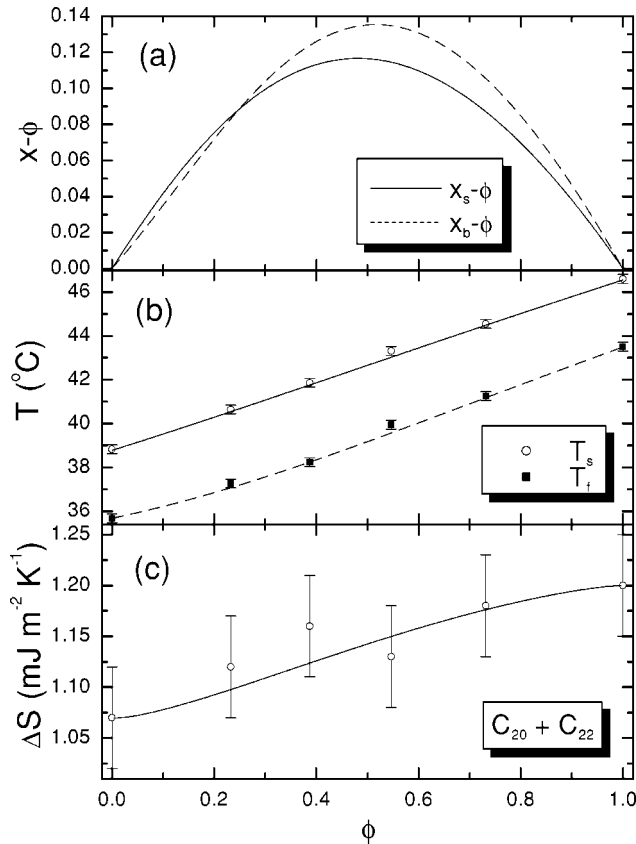


FIG. 2. Thermodynamics of $C_{20}+C_{22}$ mixtures. ϕ is the mole fraction of C_{22} . (a) The excess molar concentration of the long component in the surface (solid line) and bulk (dashed line) solid phases relative to the bulk liquid phase. Their derivation from the experimental data using a thermodynamical model is discussed in the text. (b) The surface T_s (open circles) and bulk T_f (solid squares) freezing temperatures, obtained from surface tension measurements. The fits to theory, discussed in the paper, are shown by lines. (c) The entropy loss upon surface freezing. The circles are derived from surface tension measurements. The line is the prediction of our theoretical model, based on the mole fraction differences between the solid and the liquid phases, shown in (a). The line is obtained without any adjustable parameters.

much more: $\approx 60\%$ [Fig. 3(a), dashed line]. The mismatch term in this case is large, and can dominate for certain ϕ 's. This occurs in Fig. 3(a) near $\phi \approx 0.18$, where a large, albeit still continuous, drop in x_b is observed. This curve, however, can also be interpreted as showing a jump between two constant $x_b(\phi)$ values. Figure 3(b) also shows a good fit to $T_f(\phi)$ at the edges, $\phi \rightarrow 0$ and $\phi \rightarrow 1$, but significant deviations for midrange ϕ values. A similar effect is observed in Fig. 4, where results are shown for a large Δn mixture of deuterated+hydrogenated molecules. The deviations of $T_f(\phi)$ from the fit in Fig. 4(b) are similar to those in Fig. 3(b), though here the deviations extend over a considerably larger ϕ range. Note that for these large Δn values the observed behavior can also be accounted for by the ideal solution theory discussed below with a rotator-crystal phase transition with decreasing ϕ , as shown for $C_{12}+C_{23}$ solutions [32]. For the C_{23} -D₃₂ mixture the fit to $T_f(\phi)$ [Fig. 4(b)] can

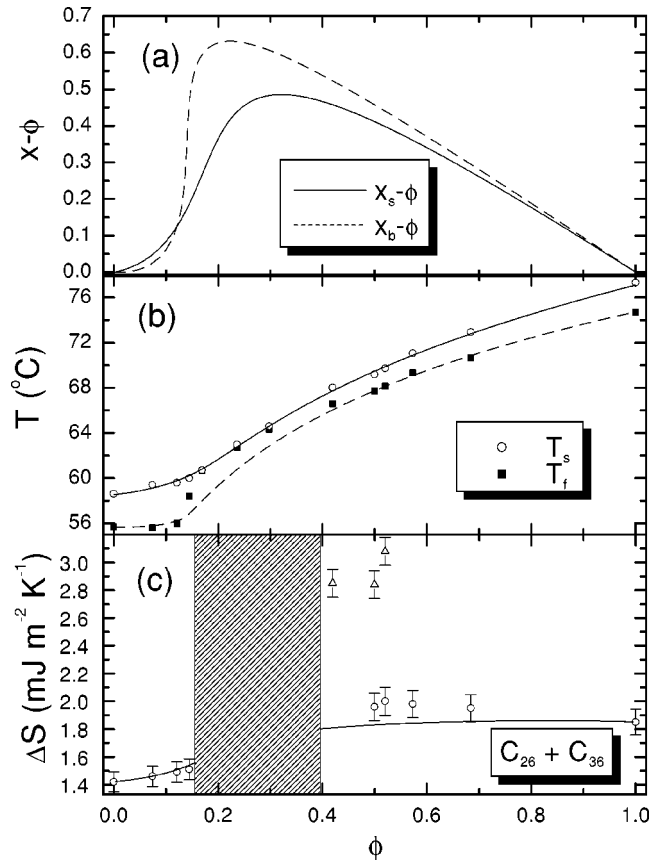


FIG. 3. Same as Fig. 2, but for the $C_{26}+C_{36}$ mixture. The shaded region in (c) is a “black hole,” where no surface freezing occurs. The high values of ΔS , shown in (c) by triangles, correspond to a different phase from that of both pure materials (circles). This phase, discussed in depth in Ref. [8], cannot be obtained from our simple theoretical model.

be improved (see dash-dotted line) by increasing the entropy of the pure components by $\sim 20\%$ above their experimental value [1,19], keeping the same interchange energy ω_b . The behavior of $x_b(\phi)$ in this case is shown in Fig. 4(a) (dash-dotted line). This behavior is not an isotope effect (which is expected to be small [11]), but rather a characteristic of all large- Δn mixtures. The need to increase $\Delta S_{n,m}^b$ *ad hoc* to achieve a better fit of the measured $T_f(\phi)$ in Fig. 4(b) (dash-dotted line), most likely reflects the anomalously high heat capacity of the rotator phase, which results in curvature in $T_f(\ln \phi)$ as ϕ decreases from unity, as discussed in the appendix of Ref. [32]. Finally, in spite of the deviations found for large $\Delta n/\bar{n}$ values, as those shown in Figs. 3 and 4, all mixtures with $\Delta n/\bar{n} \leq 0.3$ show an excellent agreement of the theory in Eq. (8) and (9) with the measured $T_f(\phi)$ values. In addition to supporting the thermodynamical theory presented above, this indicates that no significant supercooling occurs in these mixtures [33].

C. Results for the surface

For the case of surface crystallization in a binary mixture, the chemical potentials of each component in the liquid and in the crystalline *surface* phases must be equal:

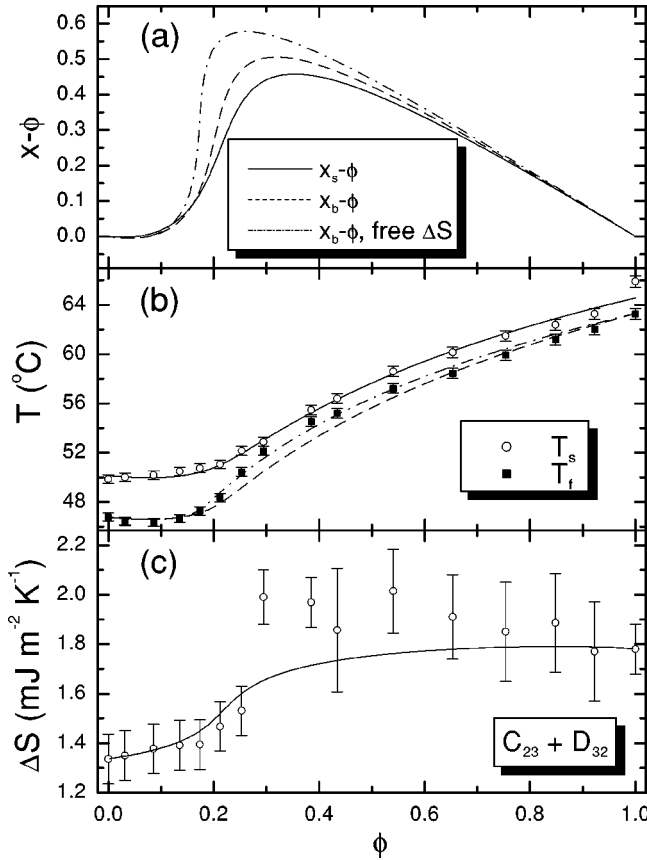


FIG. 4. Same as Fig. 2, but for the protonated-deuterated $C_{23} + D_{32}$ mixture. The dash-dotted line in (a) and (b) denotes a different calculation employing a 20% higher entropy loss upon bulk freezing for the pure component.

$$f_n^{ls} + k_B T \ln \phi^s = f_n^{cs} + k_B T \ln x_s + \omega_s (1 - x_s)^2, \quad (10)$$

$$f_m^{ls} + k_B T \ln(1 - \phi^s) = f_m^{cs} + k_B T \ln(1 - x_s) + \omega_s x_s^2. \quad (11)$$

Here the left-hand sides are the chemical potentials μ_n^{ls} (μ_m^{ls}) of the C_n (C_m) surface molecules in their liquid phase, and the right-hand sides are the chemical potentials μ_n^{cs} (μ_m^{cs}) of the C_n (C_m) surface molecules in their crystalline phase. ω_s is the *surface* interchange energy, which is generally different from ω_b used in Eqs. (6) and (7) for the bulk. ϕ^s is the mole fraction in the liquid surface phase and x_s (generally different from ϕ^s) is the mole fraction in the crystalline surface phase of the C_n molecules. These two equations for the surface are the same as Eqs. (6) and (7) used above for the bulk. The free energy difference of each component $f_n^{ls} - f_n^{cs}$ is calculated in exactly the same way as for the bulk yielding $f_n^{cs} - f_n^{ls} = (T - T_{s,n})(S_n^{ls} - S_n^{cs}) = (T - T_{s,n})\Delta S_n^s$, where ΔS_n^s denotes the entropy loss upon *surface* freezing of a single C_n molecule and $T_{s,n}$ denotes the measured *surface* freezing temperature [1,4]. Equations (10) and (11) are solved, as above, to yield for $T_s(\phi^s)$ a set of equations analogous to Eqs. (8) and (9). However, the next step, solving the equations for $x_s(\phi)$ and ω_s by fitting them to the measured $T_s(\phi)$, cannot be carried out directly, since the

liquid surface composition ϕ^s is generally different from that of the bulk ϕ due to the preferential adsorption of the lower-energy species at the surface, an effect widely known as the Gibbs adsorption rule. We use here the simplest form of this rule [34], which can be easily derived using the chemical potentials of the liquid bulk and the surface phases, given in Eq. (4) above, and some standard thermodynamics [18,25,26]:

$$\phi^s = \phi \Gamma_l / (1 - \phi + \phi \Gamma_l), \quad (12)$$

where we define the dimensionless parameter

$$\Gamma_l = \exp[(\gamma_m - \gamma_n)A/k_B T]. \quad (13)$$

γ_n (γ_m) are the surface tensions of pure C_n (C_m) components at the given temperature and $A \approx 25 \text{ \AA}^2$ is the area per molecule [18]. According to previous studies [1,4] the surface tension of a pure C_n at a fixed temperature, γ_n ($T = \text{const} > T_{s,n}$), decreases with n as $\gamma_n \propto Bn^{-2/3}$, with $B = 65.4 \text{ dyne cm}^{-1}$. Thus, Eq. (12) drives for a slight, but important, enrichment of the short chain component at the surface, i.e., $\phi^s \geq \phi$. However, the difference between ϕ and ϕ^s is small and continuous, so that the general phase behavior is the same as that of the bulk.

Equation (12) provides the necessary link allowing us to solve the equations for $T_s(\phi^s)$, obtained from Eqs. (10) and (11), by fitting them to the measured $T_s(\phi)$. This yields the solid lines in Figs. 2–4(b). As can be seen, in all cases good fits ensue. The differences between the corresponding $x_s(\phi)$ curves and the *bulk* liquid mole fraction, ϕ , are shown in Figs. 2–4(a). While no discontinuities are observed in $x_s(\phi)$, regions of steep variations occur for the larger Δn values near $\phi \approx 0.2$. If, upon increasing Δn further, a discontinuous jump occurs in $x_s(\phi)$ at this, or nearby, ϕ value, the occurrence of a rare solid-solid two-dimensional (2D) demixing transition can be expected in the surface-frozen layer. This was indeed observed recently [35].

Using the crystalline surface compositions $x_s(\phi)$ obtained from the $T_s(\phi)$ fits, one can calculate the entropy loss upon SF of the *mixture* from those of the pure components without introducing any further parameters requiring adjustments:

$$\begin{aligned} \Delta S^s = & x_s \Delta S_n^s + (1 - x_s) \Delta S_m^s + k_B \{ [x_s \ln x_s + (1 - x_s) \\ & \times \ln(1 - x_s)] - [\phi^s \ln \phi^s + (1 - \phi^s) \ln(1 - \phi^s)] \}. \end{aligned} \quad (14)$$

Here the term in the curly brackets accounts for the change in the mixing entropy of the system when the C_n molecular fraction changes from ϕ^s to x_s upon surface freezing. The agreement of this expression, which does not contain any adjustable parameters, with the values of ΔS^s derived from the slopes of the measured $\gamma(T)$ curves is good, as can be seen in Figs. 2–4(c). This further supports the applicability and validity of the simple thermodynamical theory employed above to account for the measured thermodynamical data. The shaded region in Fig. 3(c) corresponds to a region in

phase space (nicknamed “black hole”) where the SF effect does not occur, due to the preemption of surface freezing by bulk freezing, as can be observed in the corresponding T_s and T_f values in Fig. 3(b). The triangles at $0.4 < \phi < 0.55$ in Fig. 3(c) denote a different surface frozen phase, a rare transition into which was thoroughly explored in earlier studies [8,36]. That phase is of small relevance here, since here we deal only with the general behavior of the different binary alkane mixtures. Obviously, this phase, which has a different structure and entropy, cannot be predicted by our simple theoretical model. Note that the $x_s(\phi)$ values derived here are also used below to derive the layer thicknesses at various ϕ , for comparison with results obtained by x-ray reflectivity.

Finally, we note that, in principle, an expression analogous to Eq. (14) can be used to calculate the entropy loss upon freezing of the *bulk*, $\Delta S^b(\phi)$, for the mixtures. However, a comparison of this expression with experiment is not possible at present, since, to the best of our knowledge, the only measured bulk $\Delta S^b(\phi)$ values available in the literature [33] are for trivially small $\Delta n = 1, 2$, which would not provide a stringent test for the $\Delta S^b(\phi)$ expression.

D. Bulk solutions

The $C_{36} + C_m$ ($m = 18, 25, \text{ and } 26$) *bulk* $T_f(\phi)$ was found to be poorly fitted by the expressions derived from the theory above, Eqs. (8) and (9). A similarly poor fit is obtained for other $\Delta n/\bar{n} \geq 0.3$ mixtures. On the other hand, the large chain-length mismatch in these mixtures, which tends to phase-separate the components, allows them to be described as solutions rather than mixtures, i.e., substituting $x_b = 1$ in the equations above for the higher molecular weight component and $x_b = 0$ for the lower molecular weight component. As shown by Sirota [32] this eventually leads to a linear behavior of $T_f(\phi)$ in $\ln(\phi)$:

$$T_f \approx T_{f,n} + (k_B T_{f,n} / \Delta S_n^b) \ln \phi \quad (15)$$

even for ϕ values as low as 0.1. Here the subscript n denotes the pure solute component, C_{36} . If, upon changing ϕ , any solid-solid bulk phase boundary is crossed, ΔS_n^b will change, and $T_f(\phi)$ will still be linear in $\ln(\phi)$ above and below the transition, but with different slopes [32]. The $T_f(\phi)$ vs $\ln(\phi)$ behavior is independent of the thermodynamical properties of the low molecular weight “solvent,” and thus allows us to show all three solutions on the same plot in Fig. 5. As clearly seen in the figure, the bulk undergoes a phase transition at $T \approx 68.5^\circ\text{C}$, which is almost certainly a rotator-crystal transition, similar to that observed in C_{23} solutions [32]. Above the transition, the freezing occurs at a liquid-rotator equilibrium line (solid). Below the transition, the freezing occurs at a liquid-crystal equilibrium line (dashed line), which has a lower slope due to a 50% higher entropy loss upon freezing, as compared to that at a liquid-rotator transition. The intersection of the dashed line and the T axis at $\phi = 1$ yields the temperature at which the liquid-crystal transition would have occurred in pure C_{36} , if there was no rotator phase. This temperature, 73°C , is lower by 1.9°C than estimated earlier [19]. The slopes of both the liquid-rotator (solid) and the

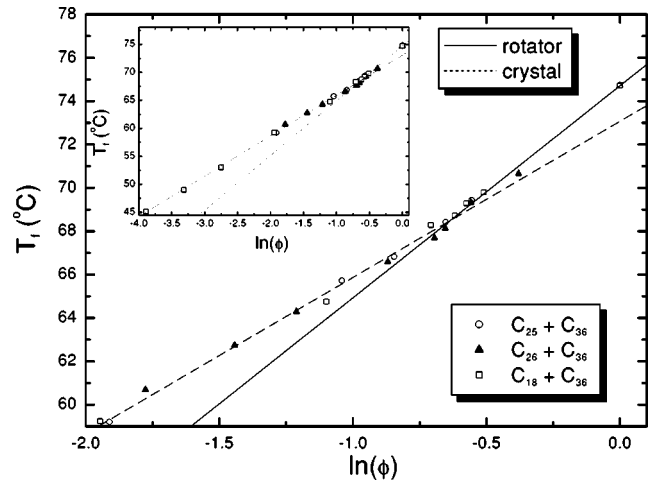


FIG. 5. The high chain-length mismatch limit: Bulk solutions. C_{36} solutions in C_{18} (open squares), C_{25} (open circles), and C_{26} (solid triangles) are shown to fall on the same line, as predicted by solutions theory. A solid-solid transition occurs in the bulk at $T = 68.5^\circ\text{C}$, as manifested by the slope change in the surface-tension-measured bulk freezing temperature data. These temperatures are linear in $\ln(\phi)$ both above and below the transition, as expected for a solution. The lines correspond to transitions to a rotator (solid) and a crystal (dashed) bulk phase. The pure material entropies used are 10–15% higher than experimentally measured. A larger-scale plot is shown in the inset.

liquid-crystal (dashed) lines correspond to ΔS_{36}^b values higher by 10–15% than the measured values of pure C_{36} [1,19]. The most probable reason for these deviations is that our freezing points are slightly supercooled. Our previous study on $C_{23} + C_{12}$ solutions [18] demonstrated that supercooling is indeed possible in solutions, although no supercooling is found in bulk pure alkanes in this n range [19]. The deviations could also be caused by inhomogeneities in the solutions, by the oversimplified description, which neglects internal degrees of freedom, etc. Finally, note that the behavior of all $\Delta n/\bar{n} > 0.3$ mixtures, including the $C_n + D_m$ ones, can be accounted for quantitatively, using the same solution theory employed above. In all cases slightly larger ΔS^b values are obtained, by about the same amount as those of the C_{36} mixtures above.

E. The interchange energy

The interchange energy parameter $\omega_{b,s}$ is due to the chain-length mismatch Δn between the molecules of the pure components in the bulk and the surface mixtures. As such, it should obviously depend on Δn . Since for long chains, the sensitivity to a mismatch cannot be the same as for the small ones, due to the finite number of gauche conformations in the rotator phase, bending, etc., it is reasonable to assume that $\omega_{b,s}$ should depend on the unitless quantity $\Delta n/\bar{n}$, where \bar{n} is the average of the two chain lengths. Expanding $\omega_{b,s}$ as a power series in $\Delta n/\bar{n}$, the constant term is of course zero, since interchanging equal-length chains does not cost energy. The first-power term must also be zero, since

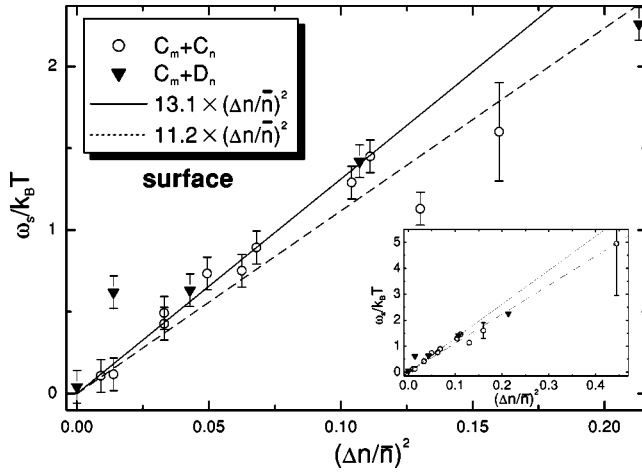


FIG. 6. The interchange energy $\omega_s/k_B T$ for the protonated-protonated (open circles) and for the protonated-deuterated (solid triangles) surface-frozen phases. Note that both fall on the same line. The inset shows the data on a larger scale. The solid line is a fit to all points with $(\Delta n/\bar{n})^2 \leq 0.12$, while the dashed line is a fit to all available points. The former is preferable, as discussed in the text.

clearly $\omega_{b,s}(\Delta n/\bar{n}) = \omega_{b,s}(-\Delta n/\bar{n})$. Thus, the first nonzero term is $(\Delta n/\bar{n})^2$. Since $\Delta n/\bar{n} \ll 1$ for all mixtures addressed here, we truncate the series after the first nonzero term. For very high $\Delta n/\bar{n} \approx 1$ phase separation will occur and the samples will anyway behave as solutions, not as mixtures. Thus, we have chosen to plot the interchange energy obtained from the fits of $T_s(\phi)$ and $T_f(\phi)$ vs $(\Delta n/\bar{n})^2$ in Figs. 6 and 7, with the insets showing the data over a larger range. For both the surface and the bulk solid phases, a linear dependence on $(\Delta n/\bar{n})^2$ is indeed found, as expected, at least for $\Delta n/\bar{n} \leq 0.3$.

For the solid surface phase, shown in Fig. 6, $\omega_s/k_B T$ can be fitted either by $11.2(\Delta n/\bar{n})^2$ (dashed line), if the full range of $\Delta n/\bar{n}$ up to ~ 0.5 is included, or by $13.1(\Delta n/\bar{n})^2$ (solid line), if only points up to $\Delta n/\bar{n} \approx 0.35$ are included. The last fit is preferable, since clearly the truncated expansion discussed above is valid only for small $\Delta n/\bar{n}$ values. At large $\Delta n/\bar{n}$ phase separation occurs and a solutionlike behavior ensues, i.e., $x_s = 0$ at low ϕ , and $x_s = 1$ at high ϕ values. At this $\Delta n/\bar{n}$ limit, the interchange energy term in the free energy has to approach zero. Therefore the error bar in the fitted $\omega_s/k_B T$ is too large to allow a clear determination of the behavior. Note that the $D_{32} + C_{32}$ mixture corresponds to zero chain-length mismatch, but may be expected to have a finite interchange energy due to the different isotopes. This “isotope mismatch” interchange energy turns out to be small, as indicated by the fact that ω_s corresponding to the $D_{32} + C_{32}$ mixture being close to zero in Fig. 6. Moreover, the ω_s values of all other deuterated-protonated mixtures, which have both a “length mismatch” and an “isotope mismatch” are equal, within the scatter observed, to the values of the corresponding protonated-protonated mixtures that have a “length mismatch” only. We conclude, therefore, that within

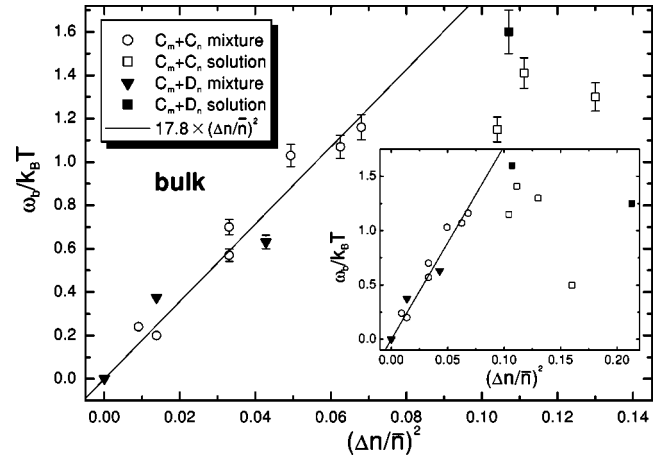


FIG. 7. The bulk interchange energy $\omega_b/k_B T$ for the protonated-protonated (open symbols) and for the protonated-deuterated (solid symbols) frozen phases. Squares denote solutions, while circles and triangles denote mixtures. The fit shown in the solid line includes all points up to $(\Delta n/\bar{n})^2 = 0.08$.

the accuracy of the present measurements the “isotope mismatch” is negligibly small.

In the solid bulk phase, Fig. 7, the linear fit in the low $\Delta n/\bar{n}$ region [$(\Delta n/\bar{n})^2 \leq 0.08$] yields $\omega_b/k_B T = 17.8(\Delta n/\bar{n})^2$. Note that despite the large differences between the sort of interactions in the quasi-2D surface solid phase and those in the 3D bulk crystal, the essential behavior of the interaction parameter remains the same. The higher constant factor (17.8 instead of 11.2) clearly means that the bulk interchain repulsive interaction is higher than that at the surface, which is reasonable since accommodating different chain lengths in the layered 3D solid induces significant strains in the structure. Moreover, the linear range of $\omega_b/k_B T$ in $(\Delta n/\bar{n})^2$ is smaller, extending to $\Delta n/\bar{n} \leq 0.3$ only. Samples having higher Δn values will undergo a bulk phase transition, as for the $C_{36} + C_{26}$, $C_{36} + C_{25}$, and $C_{18} + C_{36}$ solutions discussed above, and may show significant supercooling. In this case our mixtures theory, which assumes thermodynamical equilibrium, is inapplicable, and the solutions theory needs to be invoked. Thus, the points for $\Delta n/\bar{n} \geq 0.3$ derived from mixtures theory and shown in Fig. 7 in squares should be taken with a grain of salt. Finally, our interchange energies are of the same order of magnitude as predicted by Matheson and Smith [28]. However, a detailed quantitative comparison is not possible because of the unavailability of numerical values for some of the parameters required for their calculation.

IV. X-RAY RESULTS

The structure of the surface-frozen monolayers of the various mixtures was probed by surface-specific x-ray measurements. The x-ray results for several mixtures were discussed previously [8,36,37]. Here we concentrate on the $C_{30} + C_{36}$ mixtures as a typical example of a mixture with small $(\Delta n/\bar{n})^2 = 0.033$.

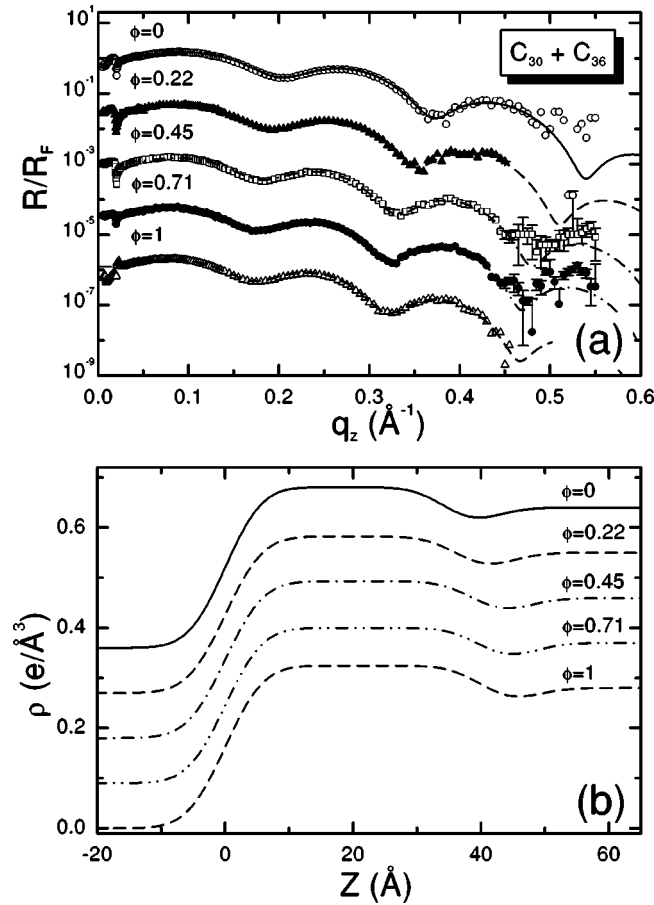


FIG. 8. (a) Measured (points) and fitted (lines) x-ray reflectivity, normalized to the Fresnel reflectivity off an ideal surface, for the surface-frozen phase of the $C_{30}+C_{36}$ mixture series. (b) The surface-normal density profiles derived from the fits in (a). The layer thickness can be seen to grow with ϕ , while the other parameters stay unchanged.

A. The surface-normal structure

Figure 8(a) shows the Fresnel-normalized x-ray reflectivities measured for different compositions of $C_{30}+C_{36}$ in their surface frozen phase. All reflectivities measured for $T > T_s$ show a monotonic fall-off typical of a liquid surface having a Gaussian roughness due to thermally induced capillary waves [1]. Below T_s , however, all five curves in Fig. 8(a) show Kiessig fringes indicating the existence of a surface layer of an electron density higher than that of the underlying liquid bulk. All five curves are similar, except for the modulation period, suggesting that the only difference is the average surface layer thickness. The fits to the two-slab model discussed above (lines) agree very well with the measured data. The thickness values derived from the fits in Fig. 8(a) are listed in Table III. In all the corresponding density profiles, shown in Fig. 8(b) the density of the $(CH_2)_{n-1}$ layer was found to be $0.316 \pm 0.006 e/\text{\AA}^3$, while the liquid bulk density was fixed at $0.28 e/\text{\AA}^3$. The roughness was found to vary around 4.7\AA and no specific trend could be identified either with ϕ or with T in the limited temperature range of existence of the surface frozen monolayer for all concentrations. All the refined parameters have very similar values to

TABLE III. X-ray GID derived data. The mole fraction x_s of C_{36} in the surface-frozen phase of a $C_{30}+C_{36}$ mixture was calculated from the measured $T_s(\phi)$ using our theoretical model. q_r is the position of the GID diffraction peak and a is the corresponding lattice spacing. The surface-frozen layer's thickness d was derived from a two-slab model fit to measured x-ray reflectivity curves.

ϕ	x_s	q_r (\AA^{-1})	a (\AA)	d (\AA)
1	1	1.494	4.856	42.08
0.71	0.88	1.495	4.852	41.95
0.45	0.67	1.502	4.831	41.01
0.22	0.34	1.503	4.826	38.45
0	0	1.504	4.825	36.22

those found for pure alkanes [1]. A monotonic growth with ϕ is found for the layer thickness, from the thickness of a pure surface-frozen C_{30} layer at $\phi=0$, to that of a pure surface-frozen C_{36} at $\phi=1$. This implies that at intermediate ϕ values both C_{30} and C_{36} must be present in the surface-frozen layer, and are most likely homogeneously mixed. In Fig. 9(b), we show (open circles) the average layer thickness values d obtained from the reflectivity fits in Fig. 8(a), for the various concentrations ϕ . The molecules in the surface-frozen phase of the pure C_{36} were previously measured by Bragg rod scans and found to have tilts of $\theta \approx 18^\circ$ from the surface normal in the nearest-neighbor direction [1]. Solving Eqs. (10) and (11) for $x_s(\phi)$ and ω_s by fitting them to the measured $T_s(\phi)$ values, as discussed above, yields an excellent agreement between the experimental (points) and the theoretical (line) $T_s(\phi)$ curves, shown in the inset to Fig. 9(b). The layer thickness can now be deduced from the $x_s(\phi)$ values obtained, shown in the inset to Fig. 9(a). Assuming the tilt of the molecules in the surface frozen phase of the mixture to be linear in the concentration x_s , the monolayer thickness of the mixture is expected to be

$$d(\phi) = [x_s d_n + (1 - x_s) d_m] \cos(\theta_n x_s), \quad (16)$$

where θ_n is the tilt of pure C_{36} and d_n, d_m are the fully extended lengths of the pure components of the surface frozen layer. Note, that assuming the tilt to be linear in x_s is just an approximation. Experimentally the tilt is known to vanish already at very low concentrations ($\sim 5\%$) of the untilted component, as discussed below. Equation (16), shown in a solid line in Fig. 9(b), agrees very well the experimental data without any further adjustable parameters, supporting the suggested molecular model for the vertical structure of the layer.

We note that the smooth variation of $d(\phi)$ observed here occurs only in mixtures with small $\Delta n/\bar{n}$. Even though the inclusion of two different-length chains in the same layer is less expensive energetically in the surface than in the bulk (due to absence of a rigid 3D lattice at the surface), for large enough $\Delta n/\bar{n}$ values the energy cost will be prohibitive. Thus, at any point on the (ϕ, T) phase diagram where surface freezing occurs a single component, pure, surface phase will be obtained, for a large enough $\Delta n/\bar{n}$ [18]. Obviously,

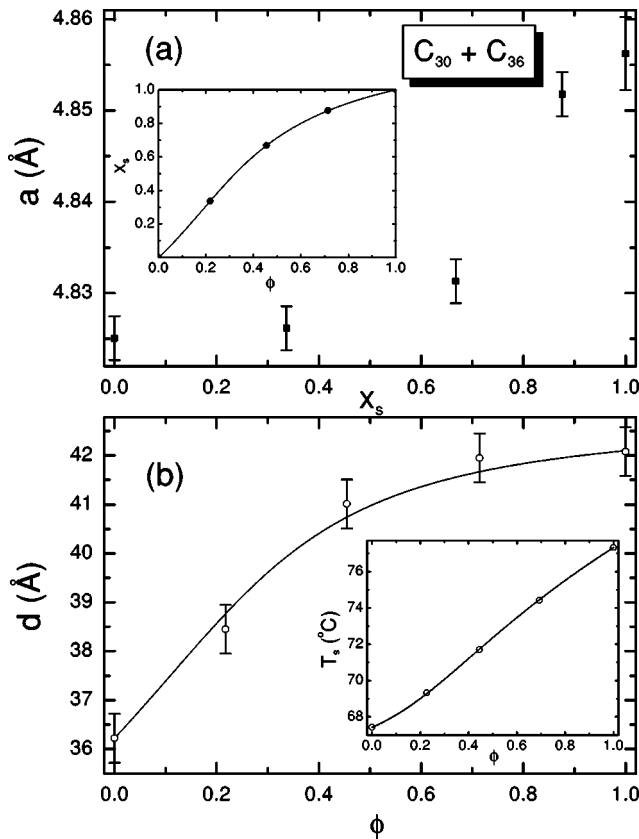


FIG. 9. (a) The lattice parameter a of the hexagonally packed crystalline surface monolayer for $C_{30}+C_{36}$. The inset shows the mole fraction x_s of C_{36} in the solid surface phase for the given liquid bulk mole fraction ϕ of C_{36} . The mole fraction x_s is obtained from a fit of a theoretical expression (line) to the measured $T_s(\phi)$ (points), both shown in the inset to (b). (b) The thickness $d(\phi)$ of surface frozen monolayer for the $C_{30}+C_{36}$ mixtures, as derived from the x-ray reflectivity measurements (points), and as calculated theoretically from the components' molecular lengths (line).

this leads to a discontinuous behavior of $d(\phi)$. Moreover, for large $\Delta n/\bar{n}$ values, the surface-freezing region may (and does) vanish for a range of nearly equimolar liquid bulk mixtures, nicknamed a “black hole.” Such a black hole is shown by the shaded region in Fig. 3(c). Finally, distinct new phases can sometimes be observed at the edge of such a black hole. A crystalline, as distinct from a rotator, surface frozen phase was observed at the edge of the black hole region in $C_{26}+C_{36}$, shown by triangles in Fig. 3(c). This phase was studied and characterized [8] and shown to be of a different structure than that of the $0.5 \lesssim \phi \leq 1$ mixtures of $C_{26}+C_{36}$. Demixing transitions, where the surface-frozen layer's composition varies abruptly between two values as the temperature is changed, are also expected to occur at the low- ϕ edge of a black hole. Such a transition was indeed observed recently in the surface-frozen phase of a binary mixture of different-length alcohols [35].

B. The surface-parallel structure

GID measurements were also carried out for the same $C_{30}+C_{36}$ mixtures used in the reflectivity measurements. As

in previous studies [8,36,37], for all samples a single in-plane diffraction peak was found at $q_r \approx 1.5 \text{ \AA}^{-1}$, indicating an hexagonal packing, with nearly surface-normal molecules. The widths of the GID peaks were resolution limited, implying an order coherence length of at least a few hundred \AA , similar to those found for pure alkanes [1,38]. The lattice spacings a derived from the peak positions for the various concentrations are shown in Fig. 9(a). The data show a significant increase in a with ϕ . However, an increase in ϕ necessarily causes an increase in T_s , as shown in the inset to Fig. 9(b), and hence also a thermal expansion of a . The increase observed in a is roughly equal to that expected from the thermal expansion, using the $7-9 \times 10^{-4} \text{ }^\circ\text{C}^{-1}$ linear thermal coefficient of expansion measured for the surface-frozen layer in alkanes [7,18,38] and $\sim 8 \text{ }^\circ\text{C}$ spread of $T_s(\phi)$ for $0 \leq \phi \leq 1$ in the inset to Fig. 9(b). An assignment of the growth in a to thermal expansion alone is, however, not tenable, since the dependence of a on the temperature T at which the GID data was taken deviates significantly from linearity. A more detailed GID and Bragg rod study would be required to separate possible lattice spacing dependence on ϕ from thermal expansion effects.

V. CONCLUSION

The surface-freezing effect was studied for binary mixtures of normal alkanes. The layer formed at the surface below T_s is found to be an ordered monolayer of surface-normal molecules, with an order coherence length of at least a few hundred \AA , very similar to the crystalline monolayer found on the surface of single component liquid alkanes [1]. For mixtures where the length difference of the two components is small, the crystalline monolayer consists of a mixture of the two components, with a concentration close to that of the bulk, and a smooth variation of the structural parameters between those of the two pure components. For a large length difference Δn , the surface crystalline monolayer is richer in the longer component than the bulk for almost all ϕ , and a noncontinuous variation of the structural parameters may occur with a variation of the bulk composition. This behavior is analogous to the bulk phase behavior: for small chain-length difference the molecules mix homogeneously, whereas for large $\Delta n/\bar{n}$ they phase separate. In cases where the surface phase consists mostly of one of the two components, the surface-frozen phase may undergo a phase transition between two compositions at a specific (T, ϕ) -space location. The overall phase behavior of the mixtures, including the transition temperatures, the entropies, the monolayer thicknesses, and the surface fraction as function of $\Delta n/\bar{n}$ and compositions, can be accounted for quantitatively using the ideal mixture theory for the liquid phase and the strictly regular mixture theory in its zeroth approximation for the solid phase. For large $\Delta n/\bar{n}$ mixtures the bulk behavior is not too well described by the strictly regular mixtures theory. While the solution theory approach provides a better description, this is achieved at the expense of introducing additional parameters, which are not known independently

and have to be determined by fitting techniques. By contrast, the mixtures theory successfully accounts for the *surface* properties of all the binary alkane mixtures measured. Moreover, the same theory is found to account well for the behavior of surface freezing in binary mixtures of normal alcohols. Our results for binary alcohol mixtures are presented and discussed in the following paper.

ACKNOWLEDGMENTS

Help by Jay Patel in the deuterated mixtures experiments is gratefully acknowledged. We thank NSLS for beam time at beam line X22B. Brookhaven National Laboratory is supported by the U.S. Department of Energy under Contract No. DE-AC02-98CH10886.

-
- [1] B.M. Ocko, X.Z. Wu, E.B. Sirota, S.K. Sinha, O. Gang, and M. Deutsch, *Phys. Rev. E* **55**, 3164 (1997).
- [2] J.C. Earnshaw and C.J. Hughes, *Phys. Rev. A* **46**, R4494 (1992).
- [3] X.Z. Wu, E.B. Sirota, S.K. Sinha, B.M. Ocko, and M. Deutsch, *Phys. Rev. Lett.* **70**, 958 (1993).
- [4] X.Z. Wu, B.M. Ocko, E.B. Sirota, S.K. Sinha, M. Deutsch, B.H. Cao, and M.W. Kim, *Science* **261**, 1018 (1993).
- [5] J.W.M. Frenken and J.F. van der Veen, *Phys. Rev. Lett.* **54**, 134 (1985); H. Dosch, T. Höfer, J. Peisl, and R.L. Johnson, *Europhys. Lett.* **15**, 527 (1991); D.M. Zhu and J.G. Dash, *Phys. Rev. Lett.* **57**, 2959 (1986); M. Elbaum and M. Schick, *ibid.* **66**, 1713 (1991); E.A. Jagla, S. Prestipino, and E. Tosatti, *ibid.* **83**, 2753 (1999); Y. Fukaya and Y. Shigeta, *ibid.* **85**, 5150 (2000); X. Wei, P.B. Miranda, and Y.R. Shen, *ibid.* **86**, 1554 (2001).
- [6] O. Gang, X.Z. Wu, B.M. Ocko, E.B. Sirota, and M. Deutsch, *Phys. Rev. E* **58**, 6086 (1998); O. Gang, B.M. Ocko, X.Z. Wu, E.B. Sirota, and M. Deutsch, *Phys. Rev. Lett.* **80**, 1264 (1998).
- [7] E. Sloutskin, H. Kraack, B.M. Ocko, J. Ellmann, M. Möller, P. LoNostro, and M. Deutsch, *Langmuir* **18**, 1963 (2002).
- [8] X.Z. Wu, B.M. Ocko, H. Tang, E.B. Sirota, S.K. Sinha, and M. Deutsch, *Phys. Rev. Lett.* **75**, 1332 (1995).
- [9] O. Gang, Ph.D. thesis, Bar-Ilan University, 1999.
- [10] T.B. Peterson, M.Sc. thesis, Northern Illinois University, 1997.
- [11] D.L. Dorset, H.L. Strauss, and R.G. Snyder, *J. Phys. Chem.* **95**, 938 (1991).
- [12] A.V. Tkachenko and Y. Rabin, *Phys. Rev. E* **55**, 778 (1997).
- [13] A.V. Tkachenko and Y. Rabin, *Phys. Rev. Lett.* **76**, 2527 (1996).
- [14] E.B. Sirota, X.Z. Wu, B.M. Ocko, and M. Deutsch, *Phys. Rev. Lett.* **79**, 531 (1997); A.V. Tkachenko and Y. Rabin, *ibid.* **79**, 532 (1997).
- [15] F.A.M. Leermakers and M.A. Cohen-Stuart, *Phys. Rev. Lett.* **76**, 82 (1996).
- [16] T.K. Xia and U. Landman, *Phys. Rev. B* **48**, 11313 (1993); M. Kawamata and T. Yamamoto, *J. Phys. Soc. Jpn.* **66**, 2350 (1997); P. Smith, R.M. Lynden-Bell, J.C. Earnshaw, and W. Smith, *Mol. Phys.* **96**, 249 (1999); M. Heni and H. Lowen, *Phys. Rev. Lett.* **85**, 3668 (2000).
- [17] G.L. Gaines, *Insoluble Monolayers at the Liquid Gas Interface* (Wiley, New York, 1966); G. Roberts, *Langmuir-Blodgett Films* (Plenum Press, New York, 1990), p. 108.
- [18] E. Sloutskin, E.B. Sirota, H. Kraack, B.M. Ocko, and M. Deutsch, *Phys. Rev. E* **64**, 031708 (2001).
- [19] H. Kraack, E.B. Sirota, and M. Deutsch, *J. Chem. Phys.* **112**, 6873 (2000).
- [20] J. Als-Nielsen and D. McMorrow, *Elements of Modern X-Ray Physics* (Wiley, New York, 2001).
- [21] J. Als-Nielsen, F. Christensen, and P.S. Pershan, *Phys. Rev. Lett.* **48**, 1107 (1982); P.S. Pershan, *Faraday Discuss. Chem. Soc.* **89**, 231 (1990); T.P. Russell, *Mater. Sci. Rep.* **5**, 171 (1990); A. Braslau, P.S. Pershan, G. Swislow, B.M. Ocko, and J. Als-Nielsen, *Phys. Rev. A* **38**, 2457 (1988); M.K. Sanyal, S.K. Sinha, K.G. Huang, and B.M. Ocko, *Phys. Rev. Lett.* **66**, 628 (1991).
- [22] M. Deutsch and B.M. Ocko, in *Encyclopedia of Applied Physics*, edited by G.L. Trigg (VCH, New York, 1998), Vol. 23, p. 479.
- [23] J. Als-Nielsen and K. Kjaer, in *Phase Transitions in Soft Condensed Matter*, edited by T. Riste and D. Sherrington (Plenum, New York, 1989), p. 245.
- [24] J.H. Hildebrand and R.L. Scott, *The Solubility of Nonelectrolytes* (Reinhold, New York, 1950).
- [25] E.A. Guggenheim, *Mixtures* (Oxford University Press, Oxford, 1952).
- [26] R. Defay, I. Prigogine, A. Bellemans, and D.H. Everett, *Surface Tension and Adsorption* (Wiley, New York, 1966).
- [27] E. Sloutskin, E.B. Sirota, H. Kraack, O. Gang, A. Doerr, B.M. Ocko, and M. Deutsch, *J. Chem. Phys.* **116**, 8056 (2002).
- [28] R.R. Matheson, Jr. and P. Smith, *Polym. Commun.* **26**, 288 (1985).
- [29] D.H. Bonsor and D. Bloor, *J. Mater. Sci.* **12**, 1559 (1977).
- [30] L.E. Reichl, *A Modern Course in Statistical Physics* (University of Texas Press, Austin, 1980).
- [31] For a theoretical treatment of this process see J.I. Lauritzen, Jr. and E. Passaglia, *J. Res. Natl. Bur. Stand., Sect. A* **71A**, 261 (1967) and J.I. Lauritzen, Jr. and E. Passaglia, *J. Chem. Phys.* **45**, 4444 (1966).
- [32] E.B. Sirota, *J. Chem. Phys.* **112**, 492 (2000).
- [33] D. Mondieig *et al.*, *J. Chem. Soc., Faraday Trans.* **93**, 3343 (1997); P.M. Ghogomu *et al.*, *Thermochim. Acta* **306**, 69 (1997).
- [34] J.H. Hildebrand and R.L. Scott, *The Solubility of Nonelectrolytes* (Reinhold, New York, 1950), pp. 406–407, Eqs. (19) and (22).
- [35] E. Sloutskin, O. Gang, H. Kraack, M. Deutsch, B.M. Ocko, and E.B. Sirota, *Phys. Rev. Lett.* **89**, 065501 (2002).
- [36] X.Z. Wu, B.M. Ocko, M. Deutsch, E.B. Sirota, and S.K. Sinha, *Physica B* **221**, 261 (1996).
- [37] X.Z. Wu, A. Doerr, B.M. Ocko, E.B. Sirota, O. Gang, and M. Deutsch, *Colloids Surf., A* **128**, 63 (1997).
- [38] B.M. Ocko, E.B. Sirota, M. Deutsch, E. DiMasi, S. Coburn, J. Strzalka, S. Zheng, A. Tronin, T. Gog, and C. Venkataraman, *Phys. Rev. E* **63**, 032602 (2001).